Military Technical College
CAIRO - EGYPT

UNSTEADY NAVIER- STOKES EQUATIONS COMPUTATION OF MANEUVERING DELTA WINGS ABOUT HIGH MEAN INCIDENCE

Osama A. Kandil * and H. A. Chuang +

ABSTRACT

In this paper, the unsteady three-dimensional thin-layer Navier-Stokes equations in the moving frame of reference are solved by using a time-accurate implicit approximately-factored finite-volume scheme. The steady results for a delta wing of aspect ratio of 1 and 20.5^{o} angle of attack are compared with the experimental data of ref. 18 . With the steay results serving as the initial conditions for the pitching motion the problem is solved. We present comparisons between the Euler equations solution and the thin-layer Navier-Stokes solution for both the steady and unsteady flows.

* Professor, Department of Mechanical Engineering and Mechanics. Old Dominion University ,Norfolk .VA 23529 USA.
+ Assistant professor , Department of Mechanical Engineering and Mechanics, Old Dominion University.Norfolk , VA , 23529 , USA.

Introduction

The literature on the computational solution and experimental data of the unsteady vortex-dominated flows, particularly in the transonic regime, is unfortunately very limited. This is attributed to the complexity of the flow and its dependence on numerous parameters, and the substantial computational cost involved for the flow resolution and the time-accurate computations.

Most of the existing unsteady computational schemes are based on the unsteady small disturbance (UTSD) theory[1-3], unsteady full potential (UFP) equation[4-6], UTSD equation with non-isentropic flow corrections[7] and UFP equation with non-isentropic flow corrections[8]. These schemes are restricted to attached flows only. For mildly separated flows, integral and finite-difference boundary-layer schemes have been coupled with potential flow schemes[9,10].

The unsteady Euler equations adequately model shock waves and their motion, entropy increase across shocks and entropy gradient and vorticity production and convection behind shocks, as can be seen from Crocco's theorem and the inviscid vorticity transport equation. Moreover, the computational solution of Euler equations adequately models separated flow from sharp edges[11-13]. For smooth-surface separation, round-edge separation, shock-induced separation, viscous diffusion and dissipation, vortex breakdown, flow transition and turbulence; viscous terms must be added to Euler equations to recover the full Navier-Stokes equations or an approximate form of these equations.

Recently, successful time accurate solutions of the unsteady Euler and Navier-Stokess equations have been presented for airfoils[13,14-17]. The only existing unsteady Euler solutions for vortex-dominated flows are those of the

rolling-oscillation of a sharp-edge delta wing in a locally conical supersonic flow around a mean angle of attack and a zero angle of attack, which were presented by the authors in Refs. 12 and 13. The authors derived the unsteady Euler equations for the flow relative motion in a moving frame of reference, and the equations have been solved by using an explicit, multi-stage time stepping, finite-volumne scheme. Periodic solutions were achieved in the third cycle of rolling oscillation. Details of the surface pressure, cross-flow velocity and cross-flow Mach contours were presented showing the primary vortex and wave shocks formation and interaction.

In this paper, the unsteady three-dimensional thin-layer Navier-Stokes equations in the moving frame of reference are solved by using a time-accurate implicit approximately-factored finite-volume scheme. The steady results for a delta wing of aspect ratio of 1 and 20.5° angle of attack are compared with the experimental data of ref. 18. With the steay results serving as the initial conditions for the pitching motion the problem is solved. We present comparisons between the Euler equations solution and the thin-layer Navier-Stokes solution for both the steady and unsteady flows.

Formulation

In the absolute frame of reference, the unsteady, compressible Navier-Stokes equations in the conservation form is given by

$$\frac{\partial \rho}{\partial t} + \nabla \cdot (\rho \bar{V}) = 0 \tag{1}$$

$$\frac{\partial}{\partial t} (\rho \bar{V}) + \nabla \cdot (\rho \bar{V} \bar{V} + p \bar{\bar{I}}) - \nabla \cdot (\bar{\bar{\tau}}) = 0 \tag{2}$$

$$\frac{\partial}{\partial t} (\rho e) + \nabla \cdot (\rho h \bar{V}) - \nabla \cdot (\bar{\bar{\tau}} \cdot \bar{V} - \bar{q}) = 0 \tag{3}$$

$$p = (\gamma-1)\left(\rho e - \frac{\rho}{2} V^2\right)$$

$$h = \frac{\gamma p}{\rho(\gamma-1)} + \frac{V^2}{2} \qquad (4)$$

$$\bar{\bar{\tau}} = \frac{2 M_\infty \mu}{Re}\left[\bar{\bar{D}} - \frac{\bar{\bar{I}}}{3} tr\,(\bar{\bar{D}})\right] \quad , \quad \bar{\bar{D}} = \frac{1}{2}\left(\bar{V}\,\bar{\nabla} + \bar{\nabla}\,\bar{V}\right) \qquad (5)$$

$$\bar{q} = -\frac{M_\infty \mu}{(\gamma-1)\,Pr\,Re}\,\nabla T \qquad (6)$$

$$\mu = T^{3/2}\left(\frac{1+C}{T+C}\right) \quad , \quad C = 0.4317 \qquad (7)$$

$$Re = \frac{\rho_\infty V_\infty \ell}{\mu_\infty} \quad , \quad Pr = 0.72 \quad , \quad M_\infty = \frac{V_\infty}{a_\infty} \qquad (8)$$

In Eqs. (1)-(8), ρ is the density, $\bar{V}$ the fluid velocity, p the pressure, e the total energy per unit mass, T the temperature, μ the viscosity, Re the freestream Reynolds number, Pr the Prandtl number, M_∞ the freestream Mach number, V_∞ the freestream velocity, and γ the ratio of specific heats. The characteristic parameters are ℓ, a_∞, ρ_∞, T_∞ and μ_∞ which are the root chord, freestream speed of sound, freestream density, freestream temperature and freestream viscosity. The Sutherland's constant C is the ratio of 198.6°R/460°R.

To express Eqs. (1)-(3) in terms of a moving frame of reference, denoted by "'", we use the following relations of the substantial and local derivatives of a scalar "a" and a vector "$\bar{A}$":

$$\frac{Da}{Dt} = \frac{D'a}{Dt'} \qquad (9.a)$$

$$\frac{\partial a}{\partial t} = \frac{\partial' a}{\partial t'} - \bar{V}_t \cdot \nabla a \qquad (9.b)$$

$$\frac{D\bar{A}}{Dt} = \frac{D'\bar{A}}{Dt'} + \bar{\omega} \times \bar{A} \qquad (9.c)$$

$$\frac{\partial \bar{A}}{\partial t} = \frac{\partial' \bar{A}}{\partial t'} - \bar{V}_t \cdot \nabla \bar{A} + \bar{\omega} \times \bar{A} \qquad (9.d)$$

where

$$\bar{V}_t = \bar{V} - \bar{V}_r = \bar{V}_o + \bar{\omega} \times \bar{r} \tag{10}$$

In Eqs. (9) and (10), $\bar{V}_t$ is the transformation velocity from the absolute frame to the moving frame, $\bar{V}_r$ the relative flui flow velocity, $\bar{\omega}$ the angular velocity of moving frame, and $\bar{r}$ is the position vector of a fluid particle with respect to the moving frame. With the transformation given in Eq. (9), Eqs. (1)-(5) become

$$\frac{\partial' \rho}{\partial t'} + \nabla \cdot (\rho \bar{V}_r) = 0 \tag{11}$$

$$\frac{\partial' (\rho \bar{V}_r)}{\partial t'} + \nabla \cdot (\rho \bar{V}_r \bar{V}_r + p \bar{\bar{I}}) - \nabla \cdot \bar{\bar{\tau}}_r = - \rho \bar{a}_t \tag{12}$$

$$\frac{\partial' (\rho e_r)}{\partial t'} + \nabla \cdot (\rho h_r \bar{V}_r) - \nabla \cdot (\bar{\bar{\tau}}_r \cdot \bar{V}_r - \bar{q}) = - \rho [\bar{V}_r \cdot \bar{a}_o + (\bar{\omega} \times \bar{r}) \cdot \bar{a}_o$$

$$+ \bar{V}_o \cdot (\bar{a}_t - \bar{\omega} \times \bar{V}_r) + \bar{V}_r \cdot (\dot{\bar{\omega}} \times \bar{r}) + (\bar{\omega} \times \bar{r}) \cdot (\dot{\bar{\omega}} \times \bar{r})] + \bar{V}_t \cdot (\bar{\bar{\tau}}_r \cdot \bar{\nabla}) \tag{13}$$

$$p = (\gamma - 1) (\rho e_r - \frac{\rho}{2} V_r^2 + \frac{\rho}{2} V_t^2)$$

$$h_r = \frac{\gamma p}{\rho(\gamma - 1)} + \frac{V_r^2}{2} - \frac{V_t^2}{2} \tag{14}$$

$$\bar{\bar{\tau}}_r = \frac{2 M_\infty \mu}{Re} [\bar{\bar{D}}_r - \frac{\bar{\bar{I}}}{3} tr (\bar{\bar{D}}_r)], \quad \bar{\bar{D}}_r = \frac{1}{2} (\bar{V} \bar{\nabla} + \bar{\nabla} \bar{V}) \tag{15}$$

where

$$\nabla_t = \nabla_o + \bar{\omega} \times \bar{r} \tag{16}$$

$$\bar{a}_t = \frac{D\bar{V}}{Dt} - \frac{D' \bar{V}_r}{D t'}$$

$$= \bar{a}_o + \dot{\bar{\omega}} \times \bar{r} + 2 \bar{\omega} \times \bar{V}_r + \bar{\omega} \times (\bar{\omega} \times \bar{r}) \tag{17}$$

In the matrix form and in terms of the Cartesian coordinate (x, y, z), Eqs. (11)-(13) become

$$\frac{\partial \hat{q}_r}{\partial t'} + \frac{\partial (\hat{E}_r - \hat{E}_{vr})}{\partial x} + \frac{\partial}{\partial y}(\hat{F}_r - \hat{F}_{vr}) + \frac{\partial}{\partial z}(\hat{G}_r - \hat{G}_{vr}) = \hat{S} \qquad (18)$$

where

$$\hat{q}_r = [\rho,\ \rho u_r,\ \rho v_r,\ \rho w_r,\ \rho e_r]^t \qquad (19)$$

$$\hat{E}_r = [\rho u_r,\ \rho u_r^2 + p,\ \rho u_r v_r,\ \rho u_r w_r,\ \rho u_r h_r]^t \qquad (20)$$

$$\hat{F}_r = [\rho v_r,\ \rho u_r v_r,\ \rho v_r^2 + p,\ \rho v_r w_r,\ \rho v_r h_r]^t \qquad (21)$$

$$\hat{G}_r = [\rho w_r,\ \rho u_r w_r,\ \rho v_r w_r,\ \rho w_r^2 + p,\ \rho w_r h_r]^t \qquad (22)$$

$$\hat{E}_{vr} = [0,\ \tau_{r_{xx}},\ \tau_{r_{xy}},\ \tau_{r_{xz}},\ u_r \tau_{r_{xx}} + v_r \tau_{r_{xy}} + w_r \tau_{r_{xz}} - q_x] \qquad (23)$$

$$\hat{F}_{vr} = [0,\ \tau_{r_{yx}},\ \tau_{r_{yy}},\ \tau_{r_{yz}},\ u_r \tau_{r_{yx}} + v_r \tau_{r_{yy}} + w_r \tau_{r_{yz}} - q_y] \qquad (24)$$

$$\hat{G}_{vr} = [0,\ \tau_{r_{xz}},\ \tau_{r_{zy}},\ \tau_{r_{zz}},\ u_r \tau_{r_{xz}} + v_r \tau_{r_{zy}} + w_r \tau_{r_{zz}} - q_z] \qquad (25)$$

$$\hat{S} = [0,\ -\rho a_{t_x},\ -\rho a_{t_y},\ -\rho a_{t_z},\ -\rho [\bar{V}_r \cdot \bar{a}_o + (\bar{\omega}\times\bar{r}) \cdot \bar{a}_o + \bar{V}_o \cdot (\bar{a}_t - \bar{\omega}\times\bar{V}_r) + \bar{V}_r \cdot (\dot{\bar{\omega}}\times\bar{r}) + (\bar{\omega}\times\bar{r}) \cdot (\dot{\bar{\omega}}\times\bar{r})] + \bar{V}_t \cdot (\bar{\bar{\tau}}_r \cdot \overleftarrow{\nabla}) \qquad (26)$$

where

$$\tau_{r_{mn}} = \frac{M_\infty \mu}{Re}\left(\frac{\partial U_{r_m}}{\partial X_n} + \frac{\partial U_{r_n}}{\partial X_m} - \frac{2}{3}\delta_{mn}\frac{\partial U_{r_p}}{\partial X_p}\right) \qquad (27)$$

$$q_m = \frac{-M_\infty \mu}{(\gamma-1)\,Pr\,Re}\frac{\partial T}{\partial X_m} \qquad (28)$$

$$\bar{V}_t \cdot (\bar{\bar{\tau}}_r \cdot \overleftarrow{\nabla}) = u_{t_n}\frac{\partial \tau_{r_{mn}}}{\partial X_m}$$

$$= \frac{M_\infty}{Re} U_{t_n}\frac{\partial}{\partial X_m}\left[\mu\left(\frac{\partial U_{r_m}}{\partial X_n} + \frac{\partial U_{r_n}}{\partial X_m} - \frac{2}{3}\delta_{mn}\frac{\partial U_{r_p}}{\partial X_p}\right)\right] \qquad (29)$$

In Eqs. (18)-(26), if $\bar{\bar{\tau}}_r$ and $\bar{q}$ vanish in the Euler limit, we obtain the unsteady Euler equations in the moving frame of reference.

Computational Method

Using the time-independent body conformed coordinate ξ, η and ζ in the moving frame of reference given by

$$\xi = \xi(x, y, z), \quad \eta = \eta(x, y, z), \quad \zeta = \zeta(x, y, z) \tag{30}$$

and using the thin-layer Navier-Stokes approximation, i.e., keeping the viscous and heat transfer derivatives in the ζ direction (normal to the body) and neglecting the ζ and η derivatives of the viscous and heat transfer terms, Eq. (18) reduces to

$$\frac{\partial' Q_r}{\partial t'} + \frac{\partial E_r}{\partial \xi} + \frac{\partial F_r}{\partial \eta} + \frac{\partial}{\partial \zeta}(G_r - G_{vr}) = S \tag{31}$$

where

$$Q_r = J^{-1} \hat{q}_r \tag{32}$$

$$E_r = J^{-1} [\xi_x \hat{E}_r + \xi_y \hat{F}_r + \xi_z \hat{G}_r] \tag{33}$$

$$F_r = J^{-1} [\eta_x \hat{E}_r + \eta_y \hat{F}_r + \eta_z \hat{G}_r] \tag{34}$$

$$G_r = J^{-1} [\zeta_x \hat{E}_r + \zeta_y \hat{F}_r + \zeta_z \hat{G}_r] \tag{35}$$

$$G_{vr} = J^{-1} [\zeta_x \hat{E}_{vr} + \zeta_y \hat{F}_{vr} + \zeta_z \hat{G}_{vr}] \tag{36}$$

$$S = J^{-1} \hat{S} \tag{37}$$

Equation (31)-(37) along with uniform flow initial conditions and the flow boundary conditions are solved using the time-accurate implicit approximate factorization which is adapted from the Beam and Warming Scheme. The boundary

conditions include the solid body conditions; $u_r = v_r = w_r = 0$, $\frac{\partial T}{\partial \zeta} = 0$, $\frac{\partial P}{\partial \zeta} = 0$, the plane of symmetry reflection condition and the inflow-outflow Riemann Invariant conditions normal to the computational boundary.

Computational Results

A sharp-edged delta wing of aspect ratio, AR, of one, at a mean angle of attack, α_m, of 20.5° and in a free stream Mach number, M_∞, of 0.3 is considered for the computational application of the implicit three-dimensional vectorized program. The body conformed grid consists of 80x38x48 cells in the ξ,ζ and η directions, respectively; and its size is one root-chord ahead of the wing vertex, two root-chords behind the trailing edge and one root-chord radius in the cross flow planes. The outer boundary consists of a hemispherical surface with its center at the wing vertex and a cylindrical surface with its axis coinciding with the wing axis. The grid is generated in cross-flow planes using a modified Joukowski transformation which is locally applied at the grid chord stations with exponential clustering at the wing surface.

Steady Flow-Euler Equations:

The implicit program is used to solve for the steady flow at 20.5° angle of attack with two levels of numerical dissipation; a low dissipation (LD) with $\epsilon_2 = 0.05$, $\epsilon_4 = 00.0025$ and $\epsilon_m = 0.25$ and a high dissipation (HD) with $\epsilon_2 = 0.25$, $\epsilon_4 = 0.0025$ and $\epsilon_m = 0.25$. Figure 1 shows the solutions at two chord stations of 0.52 and 0.81 on the wing. The figures from left to right show the surface pressure coefficient (Figures 1.1), the static pressure coefficient contours (Figures 1.2) and the cross-flow velocity directions (Figures 1.3). Here, we compare the surface pressure of the Implicit-Scheme with low dissipation with that of the experimental data of Hummel[22]. Other comparisons are given by the authors in ref. 19.

At X'/C = 0.52, the computed surface pressure with low dissipation is in excellent agreement with the experimental data. The computed static pressure contours with low dissipation show higher pressue levels than those computed contours with high dissipation, particularly in the vortical core region. With low dissipation, the highest pressure contour is 1.6, while with high dissipation the highest pressure contour (at the same location) is 1.1. Comparison of the computed surface pressure with high dissipation with that of the experimental data (given in ref. 19) shows that the computed peak suction pressure is underpredicted by 18% although the remainder of the surface pressure is in good agreement with the experimental data.

At X'/C = 0.81, the computed surface pressure with low dissipation is higher than that of the experimental data, particularly under the primary vortex core. The computed peak suction pressure is about 25% higher than that of the experimental data. Comparison of the computed static pressure contours with low dissipation shows higher pressure levels than those computed contours with high dissipation, particularly in the vortical core region. The cross flow velocities of both dissipation levels (Figures 1.3) show almost identical shapes and directions.

Figure 2 shows the experimental static pressure contours of Hummel[22] in planes perpendicular to the wind direction (Figures 2.1), the computed static pressure contours in planes perpendicular to the wing surface (Figures 2.2) and the cross-flow velocity directions (Figures 2.3). The computational results along with the experimental data are shown for two cross flow planes in the wake; X'/C = 1.02 and X'/C = 1.25. At X'/C = 1.02, the computed outer contours are in excellent agreement with the experimental contours. For the most inner static pressure contours, the experimental data show higher level than those of the computed results. On the other hand, the implicit results

with low dissipation show higher level than those of the higher dissipation. Similar results are seen at X'/C = 1.25. At this location, it is seen that the trailing-edge vortex core is captured using the low-dissipation implicit scheme.

The discrepancies between the experimental data and the computed results with low dissipation level are attributed to the grid coarseness in the vortical core and to the viscous effects in the vortex core as well as on the wing upper surface. The discrepancies between the computed results with low and high dissipation are obviously due to the low and high value of the explicit second-order damping coefficient. This case is being solved for the thin-layer N-S Equations.

Unsteady Flow (Pitching Oscillation about the Quarter-Chord Axis)-Euler Equations

The steady results with low dissipation level are used as the initial conditions for calculating the unsteady flow around the same wing which is undergoing a pitching oscillation about the quarter chord axis. The angle of attack $\alpha(t)$ is given by

$$\alpha(t) = \alpha_m + \alpha_0 \sin 2\sqrt{\gamma}\, M_\infty\, kt$$

where α_0 is the amplitude, and k is the reduced frequency ($k = \frac{k^* C}{2U_\infty}$, k^* ≡ dimensional frequency and c ≡ wing chord length). In this application α_m = 20.5°, α_0 = 2°, M_∞ = 0.3 and k = 3 which corresponds to a period of 2.95 per cycle. Each cycle of oscillation takes about 1,475 time steps and the solution covers 5,000 time steps which correspond to 3.39 cycles of oscillation. Figure 3 shows α vz t motion at the top, which is followed by the surface pressure variation, static pressure contours and cross-flow velocity in each row of figures. The numbers 1-15 on the α-t curve and on the other figures

show the instants at which the computational results are shown. Here, we show the computations at X'/C = 0.52 and the computed surface pressures are shown every 200 time steps starting from the 2,200 time step, which corresponds to point 1 on the α-t curve. The static pressure contours and the cross-flow velocity directions are given at the 3,000; 4,000 and 5,000 time steps which correspond to points 5, 10 and 15, respectively; on the α-t curve. Comparison of the surface pressure at points 7 and 14, corresponding to 2.31 and 3.25, cycles respectively, shows that periodic oscillation has already been reached. This case is being solved for the thin-layer Navier-Stokes Equations.

The full length paper covers comparisons of the steady and unsteady results with the thin-layer Navier-Stokes equations using fine grid of 80x48x58 in the ξ, ζ and η directions;respectively.

References

1. Ballhaus, W. F. and Goorjian, P. M., "Implicit Finite-Difference Computations of Unsteady Transonic Flows about Airfoils," AIAA Journal, Vol. 15, No. 12, December 1977, pp. 1728-1735.

2. Edwards, J. W., Bland, S. R. and Seidel, D. A., "Experience with Transonic Unsteady Aerodynamic Calculations," NASA TM-86278, 1984.

3. Batina, J. T., "Unsteady Transonic Algorithm Improvements for Realistic Aircraft Applications," AIAA 88-0105, January 1988.

4. Chipman, R. and Jameson, A., "Full Conservative Numerical Solutions for Unsteady Irrotational Transonic Flow about Airfoils," AIAA 79-1555, July 1979.

5. Goorjian, P. M., "Implicit Computations of Unsteady Transonic Flow Governed by the Full Potential Equation in Conservation Form," AIAA 80-0150, January 1980.

6. Ruo, S. Y., Malon, J. B. and Sankar, L. N., "Steady and Unsteadcy Full Potential Calculation for High and Low Aspect Ratio Supercritical Wings," AIAA 86-0122, January 1986.

7. Batina, J. T., "Unsteady Transonic Small-Disturbance Theory Including Entropy and Vorticity Effects," AIAA 88-2278-CP, April 1988.

8. Whitlow, W., Jr., "Application of a Nonisentropic Full Potential Method to AGARD Standard Airfoils," AIAA 88-0710, January 1988.

9. Howlett, J. T. and Bland, S. R., "Calculation of Viscous Effects on Transonic Flow for Oscillation Airfoils and Comparisons with Experiment," NASA TP-2731, September 1987.

10. Weinberg, B. C. and Shamroth, S. J., "Three-Dimensional Unsteady Viscous Flow Analysis Over Airfoil Sections," NASA CR 172368, 1984.

11. Kandil, O. A. and Chuang, H. A., "Influence of Numerical Dissipation on Computational Euler Equations for Vortex-Dominated Flows," AIAA Journal, Vol. 25, No. 11, November 1987, pp. 1426-1434.

12. Kandil, O. A. and Chuang, H. A., "Computation of Steady and Unsteady Vortex-Dominated Flows," AIAA 87-1462, June 1987. To appear in the AIAA Journal, 1988.

13. Kandil, O. A. and Chuang, H. A., "Unsteady Vortex-Dominated Flows Around Maneuvering Wings Over a Wide Range of Mach Numbers," AIAA 88-0317, January 1988.

14. Kandil, O. A. and Chuang, H. A., "Unsteady Transonic Airfoil Computation Using Implicit Euler Scheme on Body-Fixed Grid," SECTAM XIV Developments in Theoretical and Applied Mechanics, April 1988, pp. 37-46. Accepted for publication AIAA Journal.

15. Anderson, W. K., Thomas, J. L. and Rumsey, C. L., "Extension and Applications of Flux-Vector Splitting to Unsteady Calculations on Dynamic Meshes," AIAA 87-1152-CP, 1987.

16. Visbal, M. R. and Shang, J. S., "Numerical Investigation of the Flow Structure Around a Rapidly Pitching Airfoils," AIAA 87-1424, June 1987.

17. Rumsey, C. L. and Anderson, W. K., "Some Numerical and Physical Aspects of Unsteady Navier-Stokes Computations Over Airfoils Using Dynamic Meshes," AIAA 88-0329, January 1988.

18. Hummel, O., "On the Vortex Formation Over a Slender Wing at Large Angles of Incidence," AGARD CP-247, January 1979, pp. 15.1-15.17.

19. Kandil, O. A. and Chuang, H. A., "Prediction of Unsteady Loads on Manuevering Delta Wings Using Time-Accurate Euler Schemes," AIAA-88-2280-CP, April 1988.

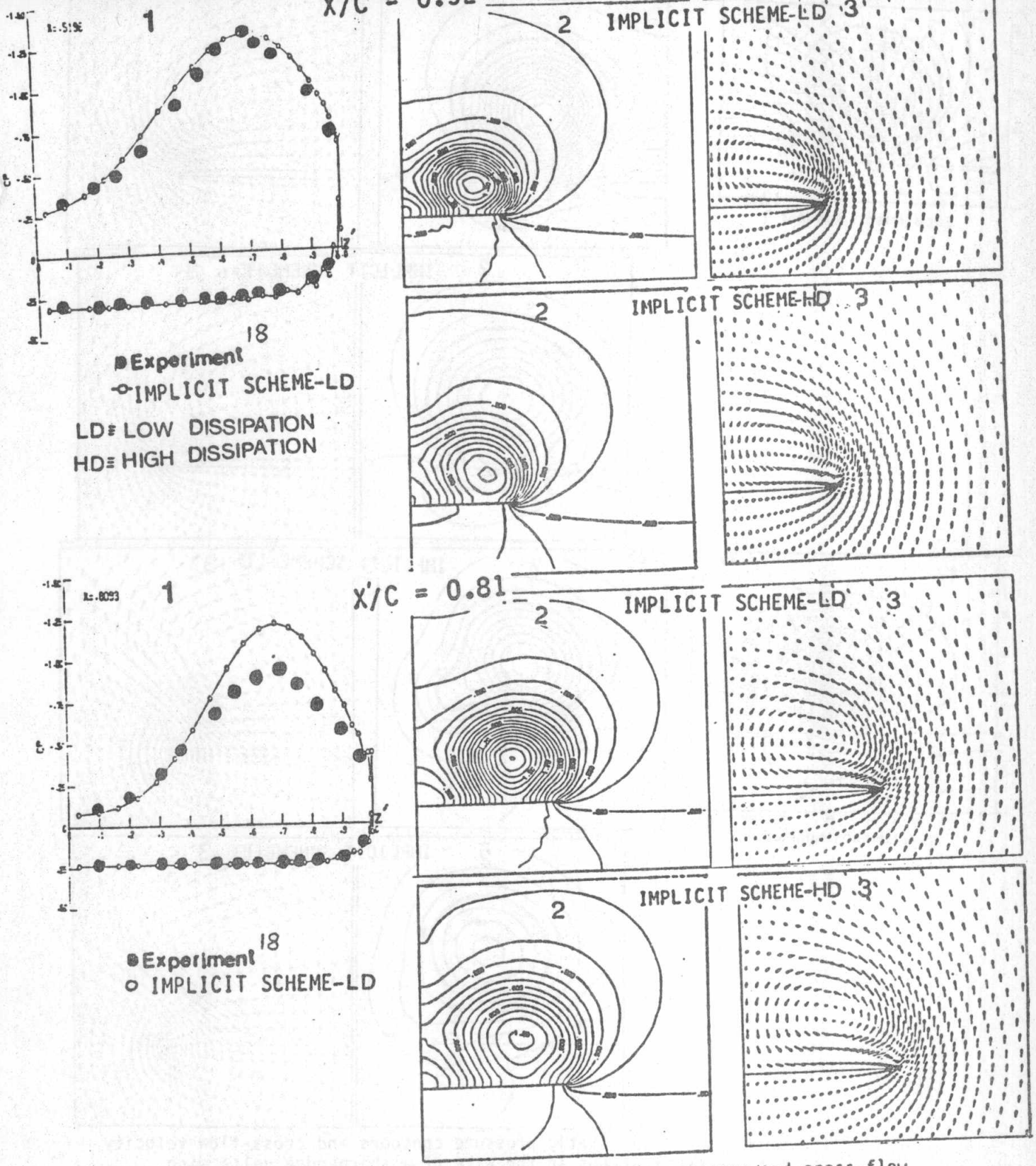

Figure1 . Comparison of the surface pressure, static pressure and cross-flow velocity at two chord stations on the wing for a sharp-edge delta wing, 80x38x48 cell, M_∞ = 0.3, α = 20.50^0, AR = 1; 1. Surface pressure, 2. Static pressure contours, 3. Cross-flow velocity.(Euler)

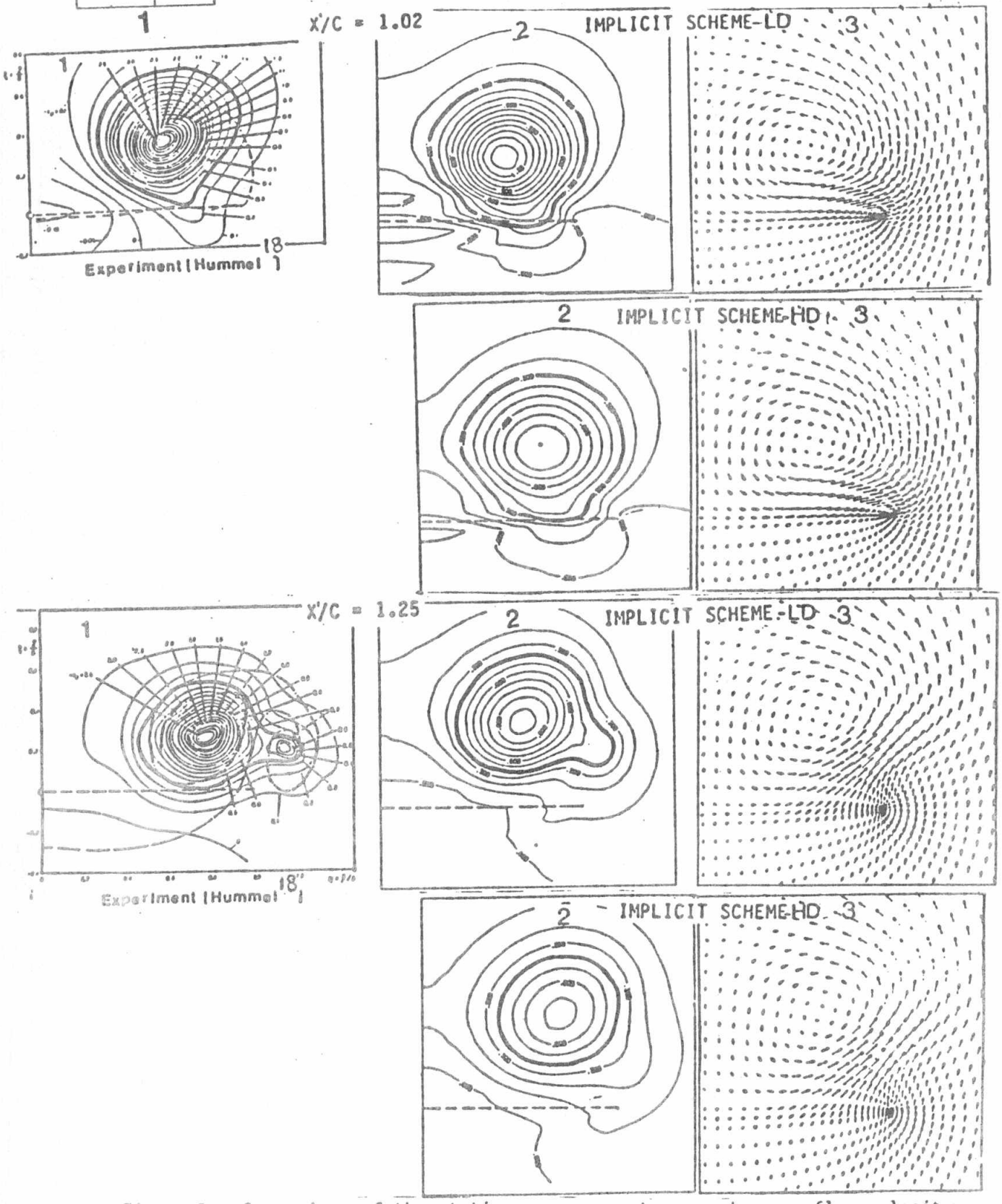

Figure 2. Comparison of the static pressure contours and cross-flow velocity at two chord stations in the wake of a sharp-edge delta wing, 80x38x48 cell, $M_\infty = 0.3$, $\alpha = 20.5^0$, Ar = 1; 1. Experimental static pressure contours, 2. Computed static pressure contours, 3. Cross-flow velocity. (Euler)

CA-6	71

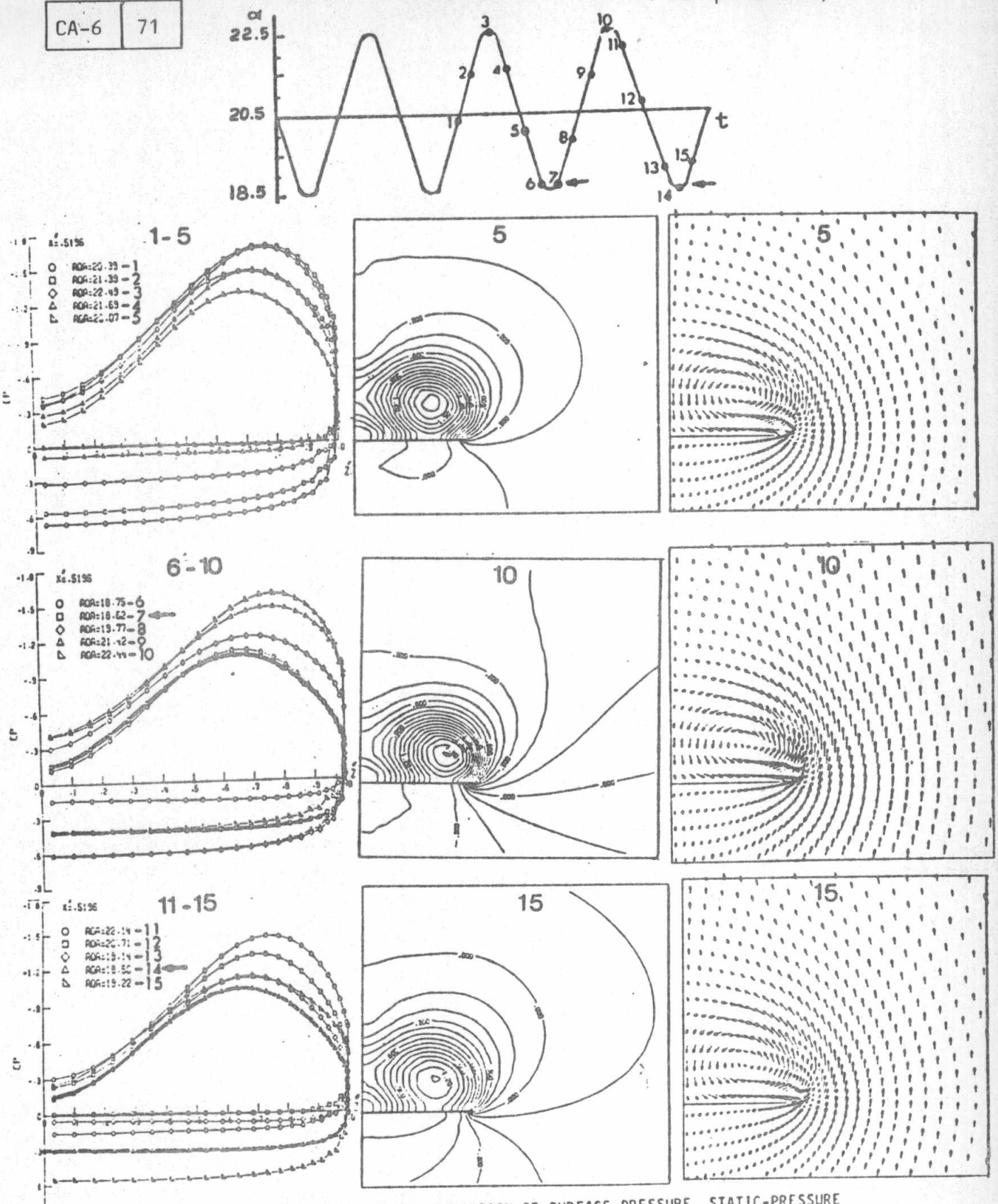

FIGURE 3. PITCHING MOTION, VARIATION OF SURFACE PRESSURE, STATIC-PRESSURE CONTOURS AND CROSS-FLOW VELOCITIES FOR A SHARP-EDGED DELTA WING UNDERGOING PITCHING OSCILLATION; 80X38X48 CELL, $M_\infty = 0.3$, $\alpha_m = 20.5^0$, $\alpha_o = 20^0$, $k = 3$, AR = 1, $\epsilon_2 = 0.05$, $\epsilon_4 = 0.0025$, $c_m^m = 0.25$. (Euler)